Pressure redistribution and free phase gas formation during and after undrained unloading of dissolved gas-charged sediment

Jason M. Abboud[1], M. Cathryn Ryan[1], Jocelyn L. Hayley[2], & Rachel M. Lauer[1]
[1]Department of Geoscience – University of Calgary, Calgary, Alberta, Canada
[2]Department of Civil Engineering – University of Calgary, Calgary, Alberta, Canada

ABSTRACT
Free-phase gas (FPG) formation and mobility in gas-saturated waters in the subsurface have geological and engineering implications, including topics as diverse as hydraulic fracturing and slope stability. FPG can form in submarine slopes and in groundwater where thermogenic or biogenic gasses are produced. Gas exsolution occurs when total dissolved gas pressure (P_{TGD}) exceeds pore water pressure (P_W), forming FPG (bubbles). We measured the responses of P_{TGD}, P_W, and volumetric water content during stepwise unloading of gas-charged sediment in a uniaxial cell filled with glass beads with varying grain sizes (2000 µm, 500 µm, 300 µm, 150 µm, 65 µm) to create FPG-water characteristic curves during FPG production of initially dissolved gas- and water-saturated materials. The transition from discrete FPG bubbles to gas mobilization occurred at higher saturation values in smaller grain size material.

RÉSUMÉ
La formation de gaz à phase libre (FPG) et leur mobilité dans les eaux saturées avec des gaz dans les eaux souterraines ont une implication dans la géologie et dans l'ingénierie, incluant des sujets comme la fracturation hydraulique et la stabilité de pente. Les FPG peuvent se former dans des pentes sous-marines et dans les eaux souterraines où sont produits des gaz thermogéniques ou biogéniques. Il y a dégagement de gaz quand la pression totale de gaz dissous (P_{TGD}) est supérieure à la pression de l'eau interstitielle (P_W), formant les FPG. Nous avons mesuré la réponse du contenu du P_{TGD}, P_W et la teneur en eau volumique pendant le déchargement progressif de sédiments chargés de gaz dans une cellule uniaxiale remplie de billes de granulométries variables (2000 µm, 500 µm, 300 µm, 150 µm, 65 µm) afin de créer des courbes caractéristiques d'eau-FPG pendant la production de FPG à partir de matériaux initiaux saturés en eau et en gaz dissouts. La transition de FPG à la mobilisation de gaz se déroule à des valeurs de saturation plus élevées dans des matières avec des plus petites grains.

1 INTRODUCTION

Free-phase gas (FPG) formation can affect slope stability and soil or rock strength. FPG can form in the saturated subsurface when thermogenic and/or biogenic gases are produced, and in gas-saturated water when temperature decreases, and/or when water pressure decreases. Previous offshore studies have noted the presence of FPG as discrete bubbles and sub-vertical chimneys in seabed floors (Sills et al., 1991). Continuous dissolved gas production can cause discrete bubbles to form, and then to increase in size, eventually to invade more than one pore space in a porous media, forming a 'continuous' PFG (Wheeler, 1988). Although total gas pressures have been estimated in lab studies (Wheeler et al., 1989), and have been used in groundwater studies (Manning et al., 2003), we are not aware they have been used in geotechnical lab experiments. Current field practices in gassy soils similarly fail to consider total dissolved gas pressure (P_{TGD}), or its relationship to pore water pressure (P_W; Roy and Ryan, 2013).

Gas exsolution occurs when P_{TGD} exceeds P_W, forming bubbles (or FPG; Manning et al., 2003; Roy and Ryan, 2010). In undrained systems, FPG formation may increase P_W, which can in turn affect effective stress, soil or rock strength, and soil or rock compressibility (Wheeler, 1988).

The 'bubbling point', also know known as the liquid-gas saturation point, the point at which FPG is formed, is defined at gauge pressure (i.e. where P_W is defined as zero at the water table) as:

$$P_{BUB} = P_{TDG} = P_W + P_{CAP} + P_{VAP} \quad [1]$$

where P_{CAP} is capillary pressure, P_{VAP} is vapour pressure (which is negligible at low temperature); all units are in pressure (e.g. atm, psi, or kPa). This equation can be re-arranged to determine P_{CAP} as a function of P_{TGD} and P_W:

$$P_{CAP} = P_{TDG} - P_W \quad [2]$$

Since P_{CAP} is challenging to measure it is rarely measured in gassy soil experiments, and P_{TDG} has been estimated but not measured in gassy soil investigations. Total dissolved gas pressure probes have been recently

applied in groundwater studies because of their ability to serve as proxies for continuous dissolved gas concentration data (McLeish et al., 2007, Roy and Ryan, 2010). These probes consist of a silicon tube membrane that is gas-permeable and water-impermeable, allowing gas to diffuse through the tubing until equilibrium is reached between the FPG pressure inside the tubing and the dissolved gas concentration outside the tubing (according to the Henry's Law constant). The silicon tubing is attached to a pressure transducer which measures the consequent FPG pressure, which is recorded by a data logger.

Although characteristic curves that describe the relationship between saturation and tension are well known in soil science (Hillel, 1982) and the unsaturated zone above the water table, to our knowledge they have not been applied to free gas production in saturated soils at formation pressures above atmospheric. Thus, our current understanding of FPG behaviour in saturated soils rely on similarities with unsaturated zone soil studies. Presently, there are no soil characteristic curves that relate saturation changed from bubble formation (i.e. due to thermogenic or biogeochemical dissolved gas production) and collapse (i.e. due to biogeochemical dissolved gas consumption and/or mobilization of FPG outside the area of interest) to porewater pressure, total dissolved gas pressure, or capillary pressure. With similar mechanisms to existing soil
water characteristic curves in mind, a conceptual model was developed to hypothesize FPG-water characteristic curves with desaturation (Figure 1).

This study measured P_{TDG}, P_W, and saturation in step-wise unloading of an undrained system to create a FPG-water retention curve similar to that shown in Figure 1 in a system that started at a pressure of 500 kPa.

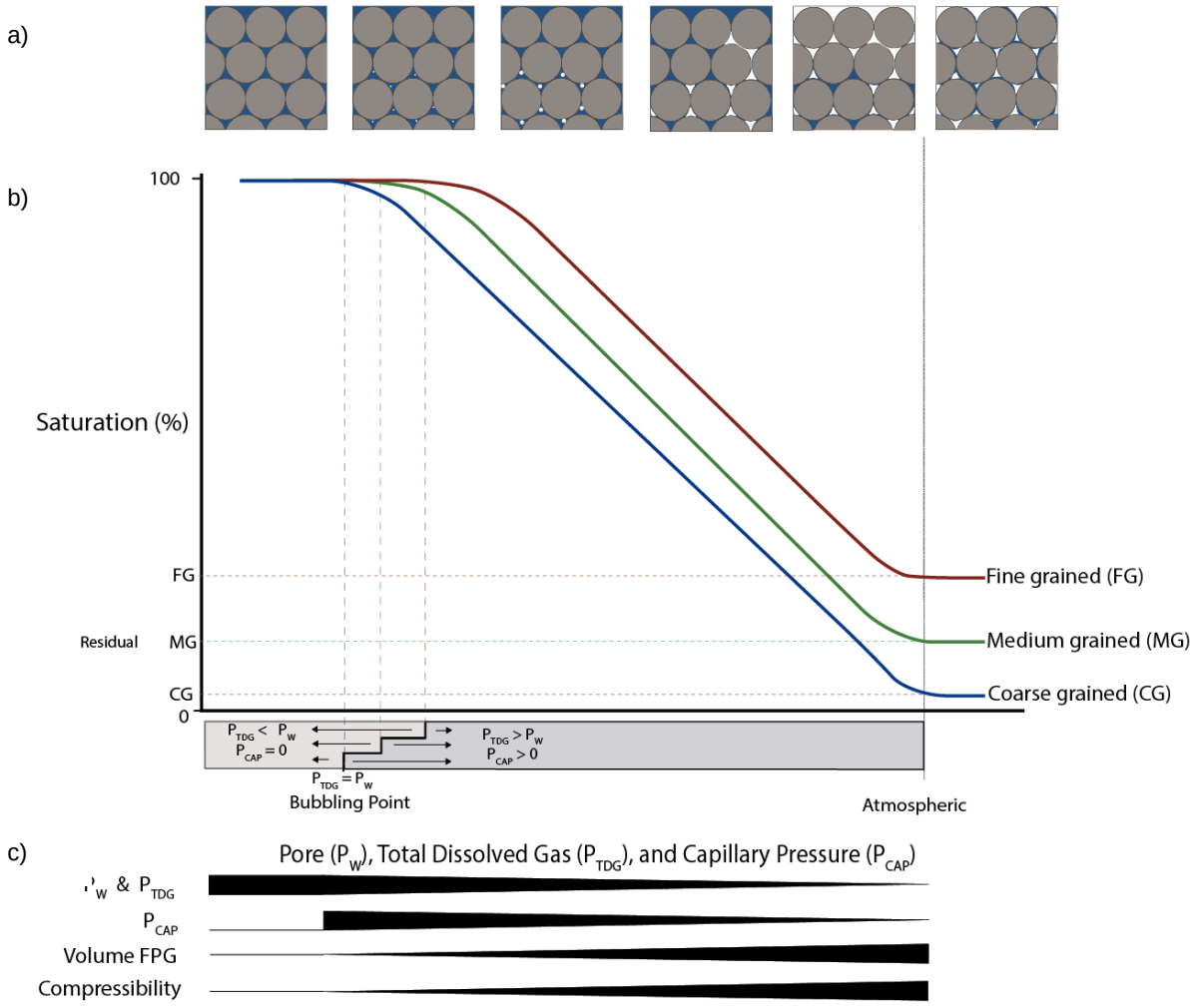

Figure 1: Free-phase gas (FPG)-water retention curves consisting of water or total dissolved gas pressure as a function of saturation. Figure a) shows bubble nucleation, mobilization, and headspace formation with desaturation. Figure b) demonstrates the effects of grain (and pore) size on desaturation with changes in total dissolved gas pressure (P_{TDG}), porewater pressure (P_W), and capillary pressure (P_{CAP}). Figure c) shows the relative P_{TDG}, P_W, and P_{CAP}, compressibility, and volume of FPG with drainage.

2 MATERIALS AND METHODS

A uniaxial apparatus (Figure 2) was used to examine pressure distribution and redistribution with step function unloading of dissolved gas-charged sediment that was allowed to equilibrate as an undrained system (with decreased total stress) after each unloading step. The apparatus included an acrylic and lexan loading cell that contained glass beads, a volumetric water content probe, and pore water pressure and total dissolved gas pressure probes. The loading cell was filled with uniform glass beads of varying sizes (Table 1).

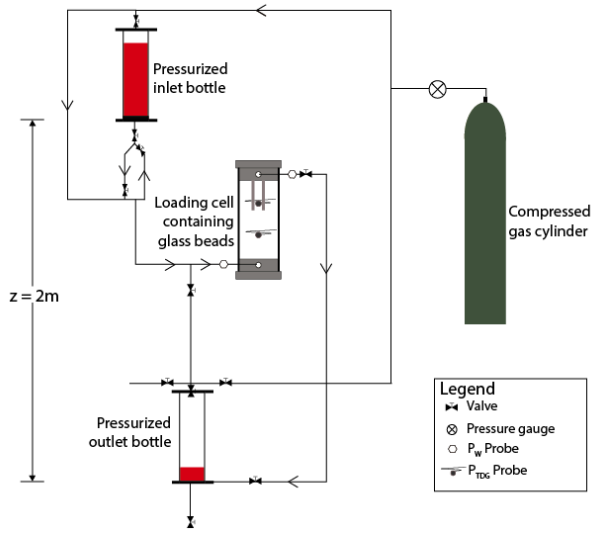

Figure 2: a) Uniaxial system set-up showing loading cell in the middle, with pressurized inlet and outlet bottles located above and below the specimen, respectively. It should be noted that there was an elevation head difference of 2 m between the inlet and outlet drainage ports (figure is not to scale). Arrows on flow lines indicate direction of flow for filling of loading cell.

Table 1: Glass bead size, soil classification, and porosities used in this experiment

Size (μm)	Soil Classification	Porosity
2000	Very coarse sand	0.33
500	Medium-coarse sand	0.31
300	Medium sand	0.31
150	Fine sand	0.29
65	Very fine sand	0.30

The loading cell was filled with rinsed and autoclaved glass beads, using a moist tamping technique. After the loading cell was filled and assembled, $CO_{2(g)}$ was run through the sample to purge atmospheric gases in the sample. Prior to the experiment, the inlet bottle (a 2.5L lexan cylinder) filled with water (with added food colouring and sodium azide as a biocide; Lichstein and Soule, 1943), and subsequently de-aired and pressurized with $CO_{2(g)}$ to ~600 kPa. After the loading cell was purged with $CO_{2(g)}$, the loading cell and an outlet bottle were filled to the same initial pressure as the loading cell. The gas-saturated water was subsequently allowed to flow from the inlet bottle and through the loading cell, saturating the cell from the bottom to the top, prior to flowing into the outlet bottle. The elevation head was the only driving force to flow gas-saturated water from the inlet to the loading cell. This slow flow rate (~1 mL/min) ensured slow saturation of the loading cell with minimized bubble formation. After approximately three pore volumes flowed through the loading cell, flow was stopped and the P_W and P_{TGD} equilibrated.

The experiments consisted of successive unloading events between which P_W, P_{TDG}, and saturation were permitted to equilibrate. Each unloading event consisted of opening the outlet port, and allowing up to 60 mL of FPG and water into a syringe, prior to shutting the port. The water and FPG volumes were estimated at near-atmospheric conditions by allowing the pressure on the syringe barrel to be released. The volumes of FPG and water in the syringe were subsequently recorded. The values of P_W, P_{TDG} and saturation were recorded until they reached steady-state values. Successive unloading events were conducted until the cell was essentially undrained and P_{TDG} was near atmospheric.

The number of total moles of CO_2 in the cell after each unloading event was estimated by subtracting the moles removed in the syringe. The latter assumed the P_{TDG} in the FPG in the syringe was near atmospheric (~ 0.88 atm in Calgary) and i) used the ideal gas law to estimate the number of moles of free phase gas n_{FPG}; and ii) combined the aqueous concentration of CO_2 (estimated using Henry's Law in equilibrium with near-atmospheric partial pressure of CO_2 in the FPG in the syringe) with the measured volume of water to estimate the number of moles of dissolved gas n_{AQ}. The total number of moles remaining in the cell were partitioned between aqueous and FPG by estimating the V_{FPG} associated with the measured saturation.

The P_W and P_{TDG} values from two probes were averaged for presentation, and saturation was measured using a TDR probe that was fitted into the lid of the apparatus.

3 RESULTS

Each unloading event resulted in a similar pattern of pressures (Figure 3). Here, P_i denotes the steady state value of P_W and P_{TDG} pressures prior to unloading. A sudden drop in P_W was observed immediately after unloading (i.e. after removing water and FPG with the syringe), then 'rebounded' to a new equilibrium value, P*eq*. The pressure lost between P*i* and P*ss* is nonrecoverable pressure, or P*nr*. The rebound period is attributed to the formation of increased FPG volume by partitioning of dissolved CO_2 into the FPG phase. The steady state P_{TDG} and P_W values are attained when FPG and aqueous equilibrium is reached, as described by Henry's Law. The equilibrium values of P_{TDG} and P_W, and saturation were recorded after each unloading event.

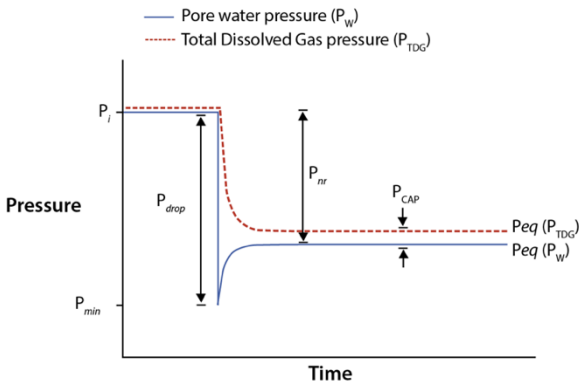

Figure 3: Schematic drawing of pore water (P_W, blue line) and total dissolved gas (P_{TDG}, red dashed line) pressures. Initial pressure indicated by P*i*, P*min* indicated minimum porewater pressure, P*nr* is nonrecoverable pressure, P*eq* is equilibrium pressure. Capillary pressure, P_{CAP}, is estimated as the difference between P_{TGD} and P_W.

Sequential unloading was conducted twice for each of five grain sizes (Table 1). A sample time series for one experiment of P_W, P_{TDG}, and saturation over 18 unloading events is shown in Figure 4 for 150 μm glass bead for an initial pressures of Pw and P_{TDG} of about 500 kPa and final pressures close to zero gauge pressure.

A saturation curve comprised of representative experiments from each grain size is shown in Figure 5. Note that each experiment is normalized to a starting pressure of 1. Generally, larger grains desaturate quicker and release more relative water by the end of the experiment (when the loading cell reaches atmospheric pressure), as seen by the higher residual saturation when P_W approaches 0.

4 DISCUSSION

The presence of FPG was noted throughout the experiment after the first unloading event. With each grain size, similar progression of FPG formation as discrete bubbles, followed by invasion of more than one pore and the mobilization of FPG, as demonstrated in Figure 5. Initially, the loading cell was fully saturated with gas-saturated water, so no FPG was present. When P_W was reduced below P_{TDG} (at an unloading event), the P_{TDG} exceeded P_W, forming free phase gases. This phenomenon is noted as bubble nucleation. As the experiment progressed, dissolved gas diffused through the pore water and into free-gas form, causing bubble expansion. Bubble invasion was noted when bubbles occupied more than one pore space. With continued unloading, continuous pathways of bubble and FPG were noted and called FPG mobilization. Finally, this mobilization ultimately led to a headspace formation and then subsequent draining of the sample.

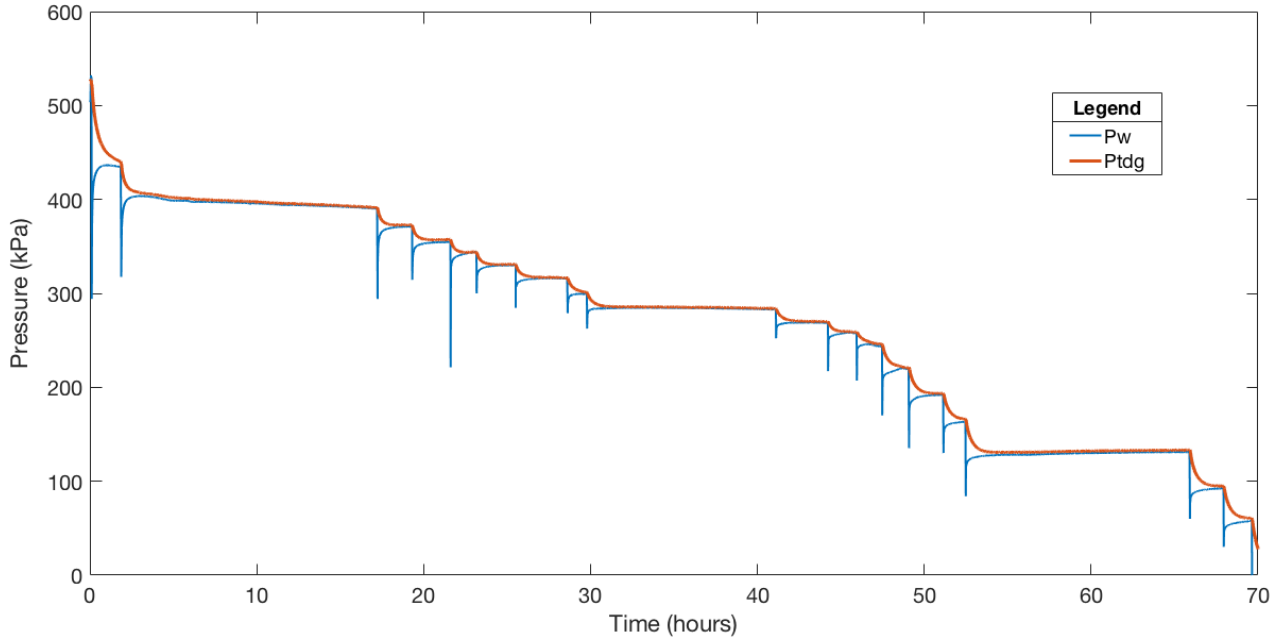

Figure 4: Example time series of P_W and P_{TGD} during 18 successive unloading events over three days for Test 1 using 150 μm glass beads. Unloading sequence for 150 μm beads. Blue line indicates pore water pressure (P_W), red line indicates average total dissolved gas pressure (P_{TDG}).

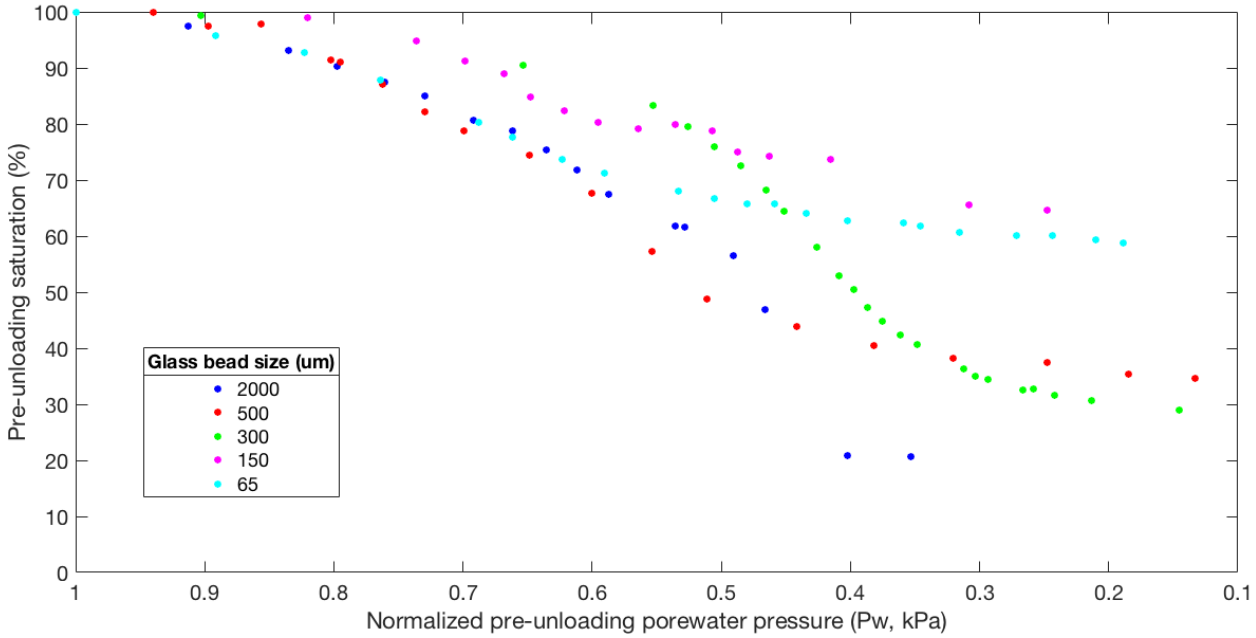

Figure 5: Saturation versus pore water pressure (P_W) curves for each grain size (2000 µm, 500 µm, 300 µm, 150 µm, and 65 µm). Each data point indicated one unloading event for the given experiment run. P_W and Saturation (%) were recorded at the beginning of the experiment and after equilibration of each unloading event.

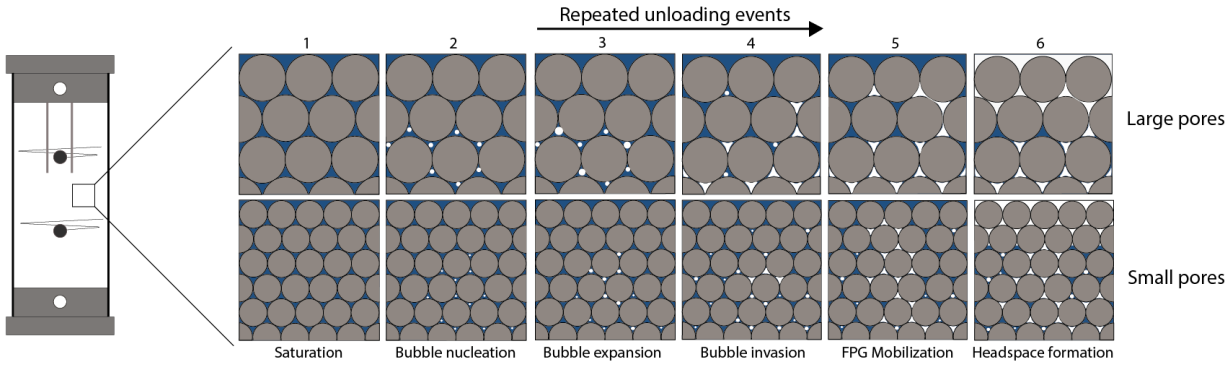

Figure 6. Schematic showing desaturation of glass beads with repeated unloading events. Progression of desaturation shows bubble nucleation (2), growth (3), invasion into more than one pore (4), mobilization after sufficient buoyancy to over come air entry pressure (not shown), and headspace formation (6). Top panel demonstrates desaturation in larger grains whereas bottom panel demonstrated desaturation with smaller grains.

Differences were seen between grain sizes, and are attributed to the differences in pore size. Smaller beads have smaller pore sizes, thus limit bubble size at nucleation and initial growth. The relationship can be demonstrated with:

$$P_{TDG} - P_W = P_{CAP} = \frac{2\sigma cos\theta}{r} \quad [3]$$

Where σ is the water-air surface tension, θ is the wetting angle, and r is the radius of curvature of the bubble.

Smaller grains have smaller pore throats, limiting the maximum size a bubble can occupy prior to invading other pores. From this equation, it can be concluded that smaller bubbles also have higher capillary pressures at bubble formation. Unfortunately, this was not measured due to equipment limitations of the uniaxial apparatus

Relationships between pore size and drainage curves are also seen in Figure 5. This phenomenon also explains the shift in drainage curves seen in water retention graphs for decreasing pore size. As hypothesized in Figure 1, different sizes of glass beads demonstrate different nucleation points. The smaller the pore size, the more energy is required for bubble nucleation. This energy is the difference between the P_W and P_{TDG}, as seen in the

above equation. Moreover, as seen in Figure 1, there would be great residual saturation for smaller beads due to the larger specific surface area of smaller beads. As the system is drained, there is a decrease in P_W, P_{TDG}, and P_{CAP} beyond the point of bubble nucleation, and an increase in the volume of FPG.

It is thought that desaturation and subsequent re-saturation of these systems with the formation and consumption of FPG, respectively, would result in hysteresis curves commonly associated with the wetting and drying of soils in the vadose zone, as suggested in Figure 7. In this case, the formation and growth of FPG is analogous to drying, and gas consumption or mobilization is equivalent to wetting of the soil. Hysteresis effects are caused when entrapped air (or FPG) delay or inhibit the equilibration during wetting or drying of the soils. Hysteresis effects due to FPG can also be accentuated with various sized pores, as larger pores drain first (upon drying) but smaller pores wet first (upon wetting).

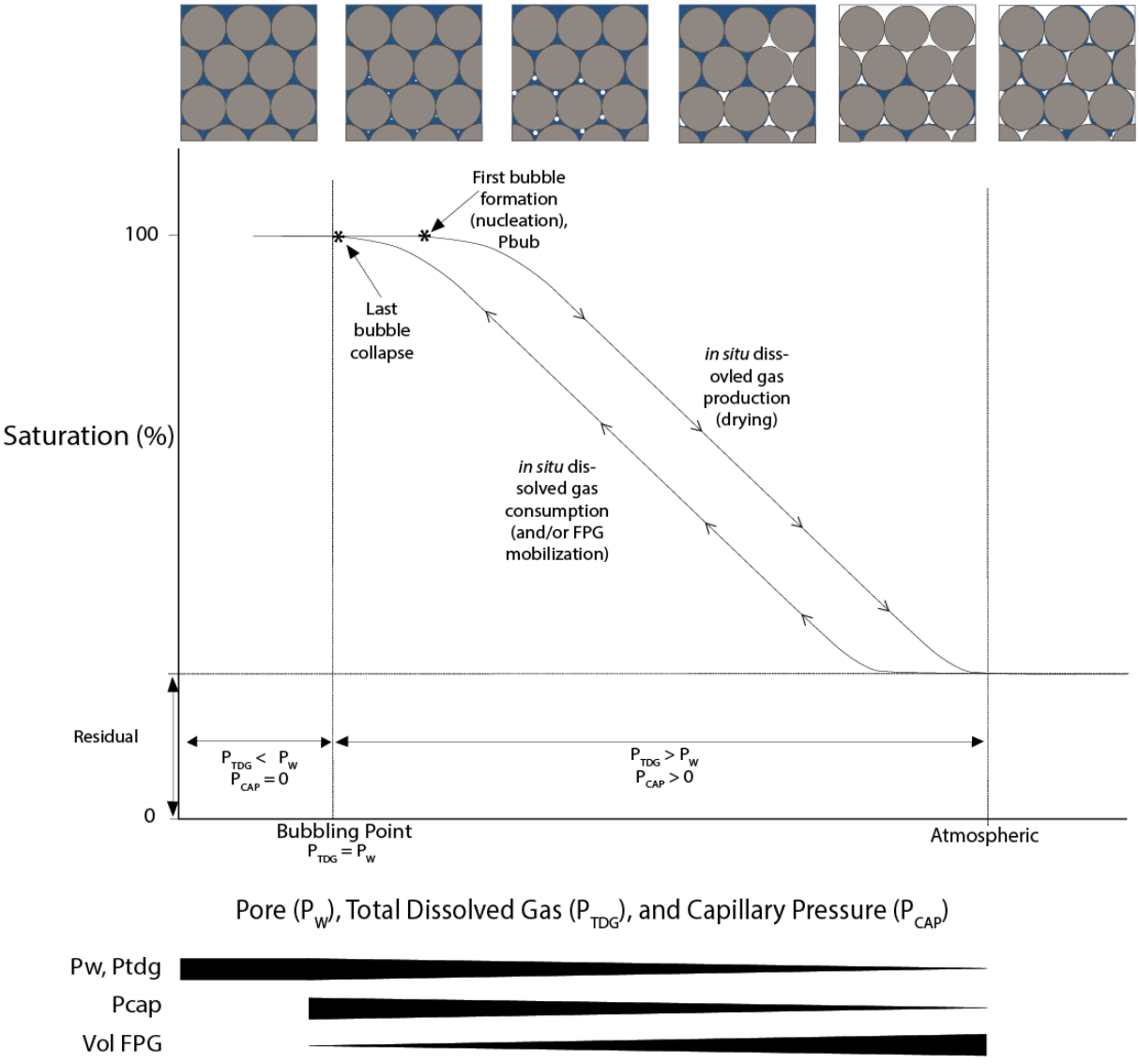

Figure 7: Water retention curves with desaturation. Figure a) shows bubble nucleation, mobilization, and headspace formation with desaturation. Figure b) demonstrates effects of grain (and pore) size on desaturation processes including bubble nucleation, residual saturation against P_{TDG}, P_W, and P_{CAP} pressures. Figure c) should relative P_{TDG},

5 CONCLUSION

This paper examined the pore water pressure (P_W) and total dissolved gas pressure (P_{TDG}) results with unloading of gas-charged sediments. Responses in P_W and P_{TDG} were recorded in successive unloading events, and were compared with different glass beads. With each unloading event, exsolution and expansions of gas (as free-phase gas, FPG) occurred after unloading of events, resulting in partial rebound of pressure loss. This partial rebound was due to the pressure applied by the FPG bubbles on to the matrix.

In comparing the water retention curves for various sizes of glass beads, it was noted that bubble nucleation occurred at lower pore pressures for smaller pores (related to P_{CAP} and r), when $P_{TDG} > P_W$ (where $P_{TDG} – P_W = P_{CAP}$). Moreover, smaller grains retain more water (specific surface area) at a given pore pressure. Finally, P_{CAP} decreases as volume of FPG increases, due to bubble expansion (Ostwald ripening) and FPG mobilization

Hysteresis effects are expected with saturation and desaturation by FPG formation and consumption. It is expected that smaller grains will also exhibit hysteresis effects similar to the ones shown, but shifted to the right.

Lastly, capillary pressure (P_{CAP}) was not measurable since it was controlled by larger diameter (2 mm) pore throats in the equipment.

Future studies can use different tubing with different diameters and thicknesses to better constrain capillary pressures. Moreover, experimental studies of desaturating and subsequent re-saturation with bubble exsolution and growth then collapse, respectively, can elucidate hysteresis effects with the presence of FPG.

6 REFERENCES

Hillel, D. 1982. *Introduction to Soil Physics*, 1st ed., Academic Press, Cambridge, MA, USA.

Lichstein, H.C. and Soule, M.H. 1943. Studies of the effect of sodium azide on microbic growth and respiration, *Journal of Bacteriology*, 47: 221-230.

Manning, A.H., Solomon D.K. and Sheldon, A.L. 2003. Applications of a total dissolved gas pressure probe in ground- water studies, *Groundwater,* 41: 440–448.

McLeish, K., Ryan, M.C. and Chu, A. 2007. Integrated sampling and analytical approach for common groundwater dissolved gases, *Environmental Science and Technology*, 41: 8388:8393.

Roy, J.W. and Ryan, M.C. 2010. In-well degassing issues for measurements of dissolved gases in groundwater, *Groundwater*, 48: 869-877.

Roy, J.W. and Ryan, M.C. 2013. Effects of unconventional gas development on groundwater: a call for total dissolved gas pressure field measurements, *Groundwater*, 51: 480-482.

Sills, G.C., Wheeler, S.J., Thomas, S.D. and Gardner, T.N. 1991. Behaviour of offshore soils containing gas bubbles, *Géotechnique*, 41: 227-241.

Wheeler, S.J. 1988. A conceptual model for soils containing large gas bubbles, *Géotechnique*, 38: 389-397.

Wheeler, S.J., Sham, W.K. and Thomas, S.D. 1989. Gas pressure in unsaturation offshore soils, *Canadian Geotechnical Journal*, 27: 79-89.